Laser and Particle Beams (2014), *32*, 569–575.

doi:10.1017/S0263034614000524

Continuous production of a thin ribbon of solid hydrogen

S. GARCIA, D. CHATAIN, AND J. P. PERIN
University of Grenoble Alpes, CEA INAC-SBT, Grenoble, France
(RECEIVED 18 June 2014; ACCEPTED 8 August 2014)

Abstract

The development of very high power laser opens up new horizons in a various field, such as protontherapy in medicine or laser-matter interaction in physics. The Target Normal Sheath Acceleration phenomenon is used in the first one. After the laser-matter impact, a plasma is generated, and free electrons move forward. It creates an electrostatic field, which can accelerate protons at the rear side of the target. The generated beam can be able to contain energetic protons with a large spectrum(1–200 MeV). This energy distribution depends on the laser power and the nature of the target. This technique has been validated by accelerating protons coming from hydrogenated contaminant (mainly water) at the rear of metallic target up to 58 MeV at Lawrence Livermore National Laboratory using the Nova Petawatt laser. However, several laser teams would like to study this interaction with pure targets. In this context, the low temperature laboratory, at CEA-Grenoble has developed a cryostat able to continuously produce a thin hydrogen ribbon (50 and 100 μm thick). A new extrusion concept, without any moving part has been carried out, using only the thermodynamic properties of the fluid. First results and perspectives are presented in this paper.

Keywords: Cryogenic target; hydrogen ribbon; proton beam

1. INTRODUCTION

Recently, the dramatic rise in attainable laser intensity by means of high power femtosecond lasers has generated a fast evolution of a new research field known as laser-driven acceleration. The production and acceleration of protons up to 60-MeV level on few micrometers are clearly visible results of this evolution (Snavely, 2000). The European project ELI will be able to produce a beam of some 10^{23} W.cm^{-2}.

The spectacular increase in brightness and decrease in pulse duration of laser-driven particle beams will revolutionize the way of investigating matter (Malka, 2008). Fundamental events in biology, femtochemistry and solid-state physics can be investigated with unprecedented space and time resolution of 10^{-15}–10^{-10}s (Malka, 2008). Moreover, great attention is devoted to medical applications of laser-accelerated light ions, especially in the hadron-therapy field (Malka, 2004).

Using present-day common laser facilities in the 100-TW power range, ions are typically accelerated from thin (∼ μm) foils up to few tens of MeV energy per mass unit. Such beams show a very low-emittance (below 10^{-2} mm mrad for protons above 10 MeV, which is 100 times better than typical RF accelerators) and extremely high ion current (kA range) (Cowan, 2004). Typically, conversion efficiencies (ratio between the laser energy and the total ion beam energy) up to 4–15 percents are measured (Brenner, 2014; Green, 2014).

Various physical mechanisms of laser-driven ion acceleration have been investigated to date. The mechanism most investigated experimentally is the Target Normal Sheath Acceleration (TNSA) when ions are accelerated at the rear side of a thin target in a quasi-electrostatic sheath formed by fast electrons propagating from the target front side (Hatchett, 2000; Maksimchuk, 2000; see Fig. 1). Usually, protons from surface impurities on metal foils (hydrocarbons) are preferentially accelerated as their charge-to-mass ratio is the highest among all ion species, thus no screening effect is present. Nevertheless, the concentration of such impurities strongly depends on the environmental conditions thus causes large fluctuations in the proton current which make laser-accelerated beams not suitable for applications. In this paper, we propose to investigate experimentally new target geometries able to produce reliable and more stable laser driven ion sources for applications. Our scheme is based on the use of an advanced cryogenic system producing pure solid hydrogen target which allows minimizing the fluctuations in the produced proton current. For this purpose, a cryostat has been developed with a specific design of an apparatus capable to deliver the required targets to a high vacuum chamber.

Address correspondence and reprint requests to: Stephane Garcia, CEA/DSM/INAC/SBT/LCF, 17, rue des Martyrs, Bâtiment D1 – Bureau 318, 38 054 Grenoble Cedex 09, France. E-mail stephane.garcia@cea.fr

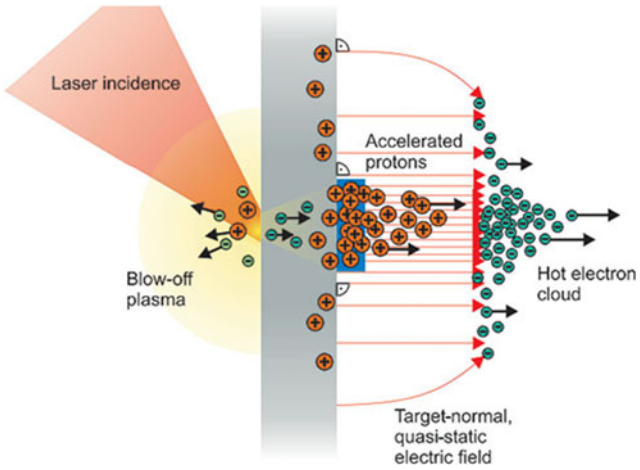

Fig. 1. Sketch showing the TNSA principle. An hot electron cloud is generated at the rear of the target, creating an electrostatic field which accelerates the protons.

The construction of new high power laser facilities (e.g., high repetition rate petawatt-class lasers as ELI-Beamlines) will clearly enable numerous prospective applications based on secondary sources of energetic particles. In particular, the use of the proposed solid hydrogen cryogenic target along with these emerging laser technologies will allow demonstrating future medical applications such as hadron therapy (Ledingham, 2007; Margarone, 2013).

The cryostat developed by the low temperature laboratory of the CEA-Grenoble, in France, enables to produce a continuous film of solid H_2 of some tens of microns in thickness and one millimeter in width. A new extrusion technique is used, without any mobile part. Thermodynamic properties of the fluid are used to make the pressure rise in a cell and push the solid H_2 through a calibrated nozzle.

2. PRINCIPLE OF SOLID FILM EXTRUSION

As discussed above, the solid hydrogen film target production is realized by a new extrusion process, developed at CEA Grenoble. In this one, no moving part is used to apply the required pressure for the extrusion. The main principle is based on the use of the thermodynamic properties of the fluid. As presented in Figure 2, the experimental cell is equipped with two heat exchangers, one situated at its top and the other one situated at its bottom, enabling to achieve the required temperatures at theses points.

The working principle of the cell is the following:

- First, when the cell is under vacuum, the temperature of the heat exchanger E1 is regulated below the triple point of the gas (i.e. 13 K for hydrogen) and the temperature of the heat exchanger E2 is regulated above (typically 20 K for hydrogen).
- Figure 2A: The Valve V1 is opened; hydrogen is introduced in the cell and immediately condenses and blocks the extrusion nozzle.
- Figure 2B: the cell is completely filled with liquid hydrogen (the temperature T2 is regulated above the triple point).
- Figure 2C: The temperature T2 is decreased slowly below the triple point to have a cell completely filled with solid.
- Figure 2D: The valve V1 is closed.
- Figure 2E: The temperature T2 is increased, the pressure in the cell rises, the temperature T1 is regulated close to the triple point and some solid is extruded through the nozzle.

By precisely controlling the temperature of T1 and T2 one can control the solid extrusion velocity at a value close to 10 mm/s. The solid film then evaporates under the effect of heat radiation and is pumped with a vacuum pump. This system was the object of a patent deposited by our laboratory.

3. EXPERIMENTAL SETUP

As shown in the Figure 3, the cryostat contains a cell surrounded by a thermal shroud at 60 K to hit radiation load heat. A burst disk prevents the cell if the pressure rises over than 20 MPa. A 200 $L.s^{-1}$ turbo molecular pump allows maintaining the cryostat under vacuum (10^{-6} mbar). The three heat exchangers of the cell and the thermal valve are cooled with helium coming from a 100 or 250 liquid liter tank. Four flow control valves are used to adjust the helium flow in each heat exchanger. Some heaters are used to adjust the required temperature of each part. The cryostat is equipped with several viewports to be able to observe the solid Hydrogen film at the outlet of the nozzle (Fig. 4). The observation can be done according to two perpendicular directions. For the moment, the solid film hydrogen, is extruded in a box which is pumped by a 35 m^3/h scroll pump which keeps the pressure around 10^{-1} mbar (depending of the Hydrogen film velocity). This box was mandatory because, as it is discussed later, we did not have a pumping apparatus allowing to maintain a sufficient low pressure in the cryostat (this pressure must be lower than 10^{-3} mbar to avoid heat transfer by convection/conduction between the vacuum vessel and the cell) during solid hydrogen extrusion. When experiences will be performed in lasers vacuum vessel, this box and all the windows will be suppressed because turbo molecular pumps of 2000 $L.s^{-1}$s will allow obtaining the required pressure in the vacuum vessel.

3.1. Required Pumping Means during Extrusion

As the solid hydrogen film sublimates, to insure the laser experiment, the vacuum level of the experimental chamber has to be maintained at a pressure lower than 10^{-4} mbar. To achieve such requirement, the sublimated solid has to be

https://doi.org/10.1017/S0263034614000524 Published online by Cambridge University Press

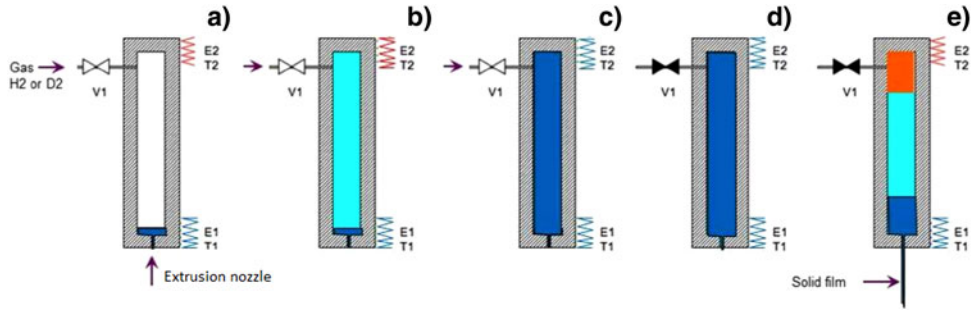

Fig. 2. Sketch showing the solid film extrusion principle.

pumped. The pumping speed of the vacuum system is given by the following equation:

$$Q = \frac{S * V * \rho_{sol} * 22.4}{M * P}. \quad (1)$$

Where Q is in l/s at standard conditions for temperature and pressure, S is the area of the solid hydrogen film (in m^2), V is the film velocity (in m/s), ρ_{sol} is the density of the solid film (in kg/m^3) M is the molar mass (in kg/mol) and P is the required pressure in the vacuum vessel (in bar). Example: for a H_2 solid film of 1 mm × 100 μm having a velocity of 10 mm/s, if the required pressure in the vacuum vessel is 5×10^{-5} mbar, one needs a 5000 $L.s^{-1}$ pump.

3.2. Required Pressure for Extrusion

To extrude through a nozzle, a solid of thickness e, width L and height H (Fig. 5), the required pressure P_e is given by the following equation:

$$P_e = \frac{2(e + L) * H * \sigma}{e * L}. \quad (2)$$

Where σ is the limit shearing stress. This value, depending on the temperature, is given by Leachman (2010) in Figure 6 for hydrogen, deuterium and neon.

For example, in case of hydrogen at 12 K, σ ~ 50 kPa, if $H = 2$ mm and $e = 10$ μm we find an extrusion pressure of 20 MPa. This pressure is easily achievable because, as shown in Figure 7 (doted line), we can see that if we fill the cell with solid at a pressure of 1 MPa at 12 K, the pressure rises to 20 MPa if the cell is heated at 20 K after having closed the filling valve of the cell.

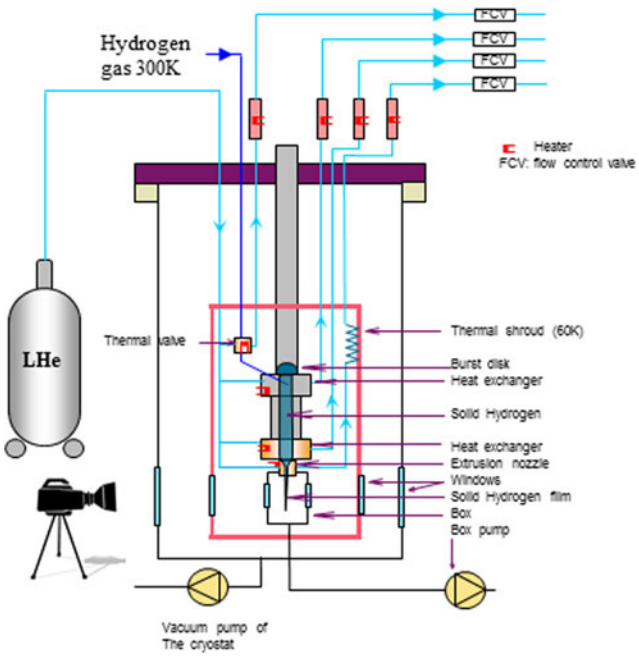

Fig. 3. Scheme of the cryostat.

Fig. 4. Cryostat Sophie II at CEA Grenoble.

https://doi.org/10.1017/S0263034614000524 Published online by Cambridge University Press

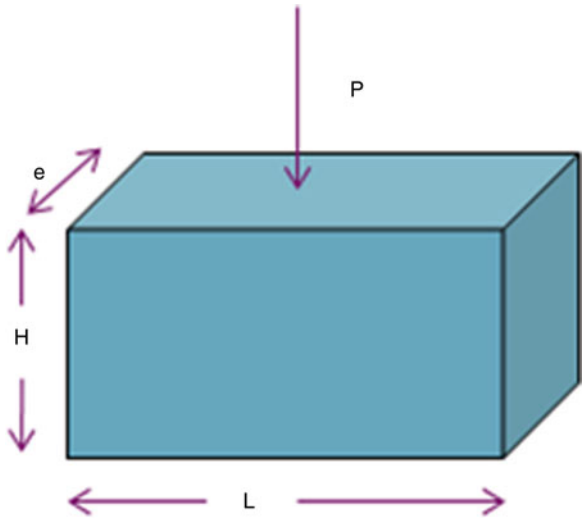

Fig. 5. Description of the applied force on the sheared solid hydrogen.

3.3. Required Time to Solidify all the Volume of Hydrogen

Before closing the filling valve of the cell (V1 in Fig. 2), we must be sure that all the volume of the cell is well solidified otherwise the pressure in the cell would not rise as we want. For this reason, we have modeled the cell and calculated the solidification time.

Figure 8 shows isotherm lines in the cell after a filling time of 25 minutes. Assuming a steady state, it enables to get the solidification front. The cell is considered filled when the top right edge's temperature is below the solidification point: no more hydrogen can enter in it.

The dark blue part corresponds to temperature below the solidification point (14.6 K at 10 bar) whereas the light blue corresponds to temperature above (up to 15.1 K). The red zone represents edges of the steel cell. The filling and solidification time depend on the temperature evolution imposed on the top of the cell by an heat exchanger. Increasing the filling time enables to rise up the solidification line, and thus to put more hydrogen in the cell.

3.4. Characterisation of the Target

The characterization of the ribbon is currently realized by two cameras placed at the front and the side view of the target (see Figs. 4 and 9). The H_2 ribbon is transparent. Preliminary measurements using an ombroscopy method show that for a given ribbon velocity, the thickness is constant all along the observed field (4×9 mm^2 for the front view and 2×4 mm^2 for the profile view). The velocity is measured by an image cross-correlation method. Other techniques are in study to get a more precise measurement of the thickness and the roughness of the target.

4. EXPERIMENTAL RESULTS

First ribbon 1 mm × 100 µm and 1 mm × 50 µm sized have been obtained. Figure 9 shows such a ribbon. The extrusion was realized continuously during 7 hours.

4.1. Relation between the Temperature of the Cell and the Pressure

The pressure of the gas (drawn in orange in Fig. 2) has to be maintained constant. To reach this requirement during extrusion, the gas above the solid part has to be heated up, following the perfect gases law: since the gas volume decreases, the temperature has to be increased to keep a constant pressure. The initial mass (m) of hydrogen contained in the cell is of importance for the extrusion behavior. Indeed, as shown in the Figure 10, obtained using hydrogen properties and equation of states, as the initial filling of the cell increases, the needed temperature for the top of the cell decreases to achieve a given pressure. Moreover, the less the initial filling, the higher the temperature gradient between two given pressures.

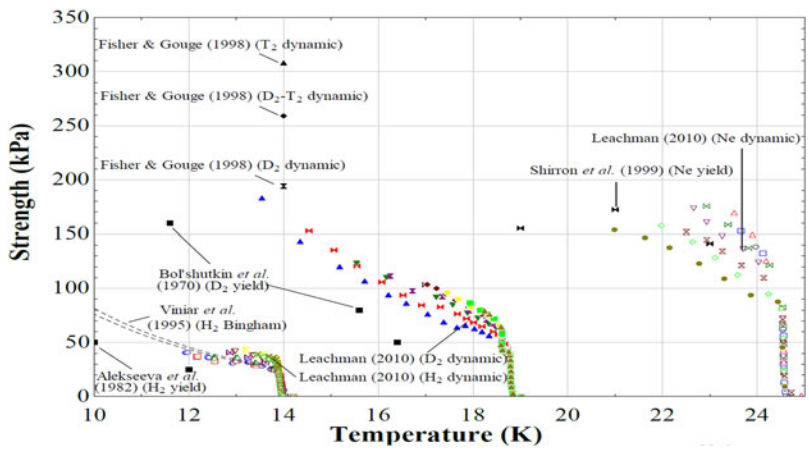

Fig. 6. Curves of limit strength of hydrogen, deuterium, and neon.

https://doi.org/10.1017/S0263034614000524 Published online by Cambridge University Press

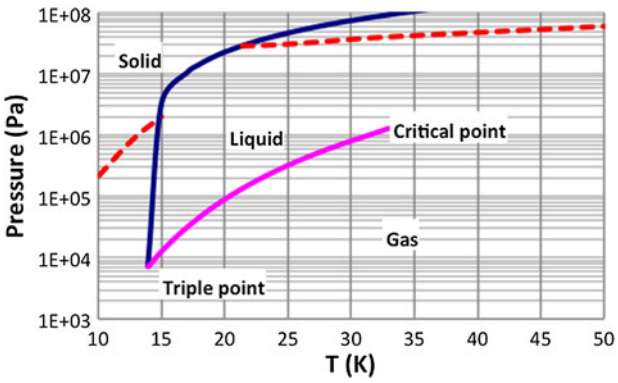

Fig. 7. Phase diagram of hydrogen—blue and pink line are respectively solid/liquid and liquid/gas limits—the red dotted curve is an isochore line.

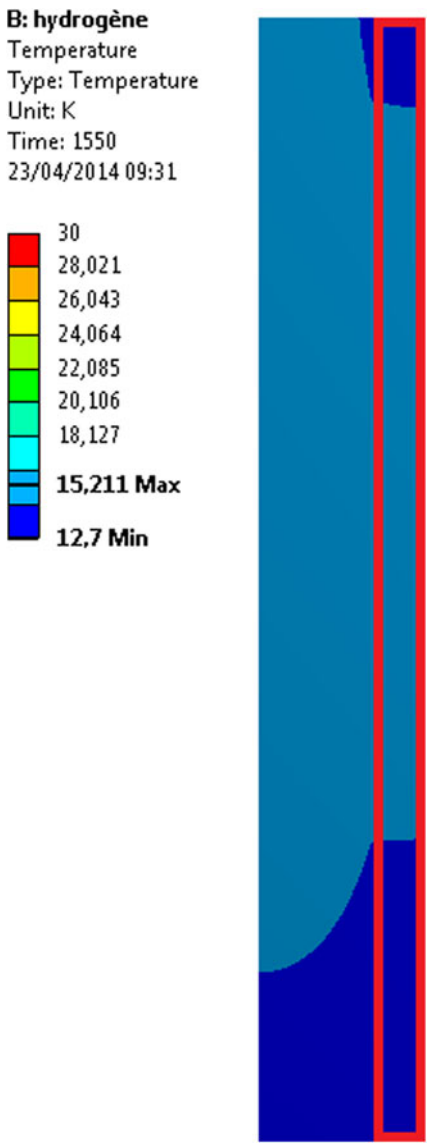

Fig. 8. 2D-axisymetric representation of the solidification line for a filling time of 25 minutes. Red zone represents edges of the steel cell.

4.2. Influence of the Nozzle Temperature on the Hydrogen Film Velocity

Experiments have been carried out to study the influence of the temperature at the extrusion nozzle T_{nozzle}, the temperature at the bottom of the cell (T), and the applied pressure inside the cell for the 100 μm nozzle as shown in Figure 11.

As the temperature on the bottom of the cell decreases, the needed pressure to achieve a given velocity increases. It is in total agreement with Figure 6, which shows that the lower the temperature, the higher the shearing stress, and thus the needed pressure to extrude.

The temperature difference between the bottom of the cell (T) and the extrusion nozzle T_{nozzle} seems to have a larger influence for low temperatures of the nozzle (11.5 K) than for higher one (12.5 K), due to the shearing stress gradient $\frac{d\tau_0}{dT}$, shown in Figure 6. Here also, the higher the temperature of the bottom, the lower the needed pressure for a given velocity

4.3. Influence of the Pressure on the Hydrogen film Velocity

Figure 11 also shows that for a given themperature on the bottom of the cell, the higher the pressure, the higher the

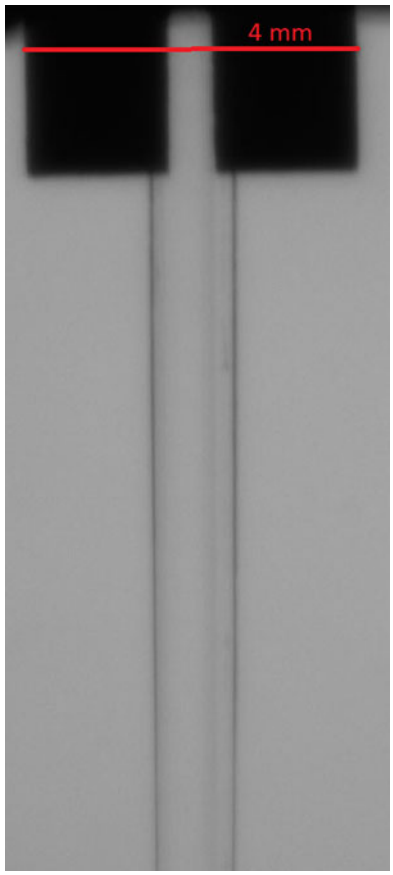

Fig. 9. Snapshot of the front view of hydrogen ribbon during extrusing through an extrusion nozzle 100 μm large.

https://doi.org/10.1017/S0263034614000524 Published online by Cambridge University Press

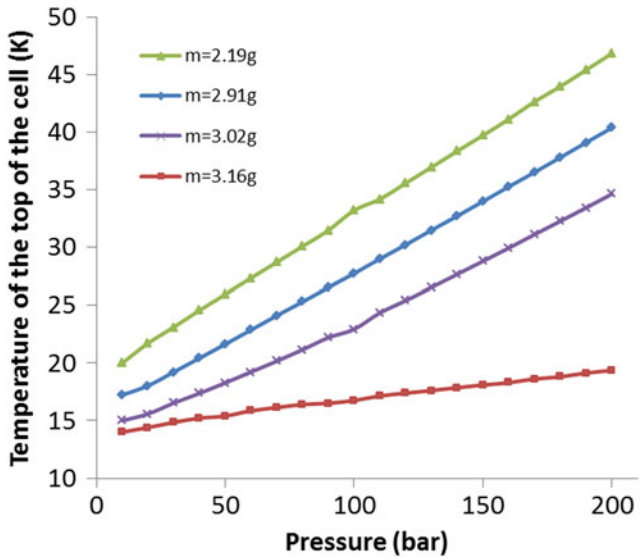

Fig. 10. Pressure-temperature relation into the cell for different initial fillings (m).

velocity, which is the expected behavior. It also shows that there is a minimum threshold, which depends on the temperature, to achieve before the solid starts to be extruded.

5. NEXT STEP

The development has been done with a 100 µm nozzle, but the extrusion nozzle has already been replaced by a 50 µm one and will be replaced by smaller ones, to obtain thinner hydrogen ribbons (25 µm and then 10 µm thick) and to establish a precise rheological behavior of the solid during extrusion.

Finite elements simulation will also be carried out to compare this model with the bibliography (Vinyar,2000; Leachman, 2010).

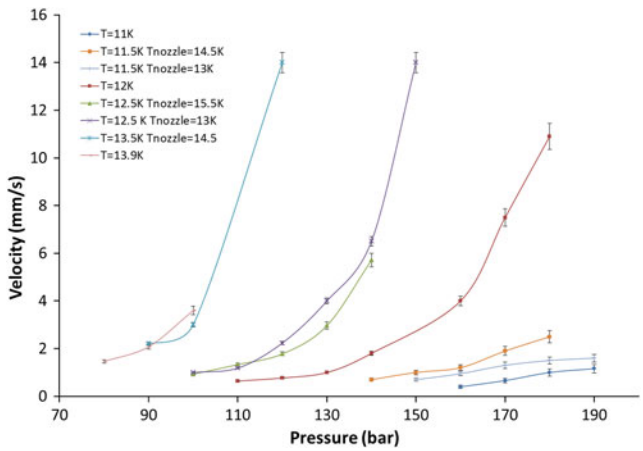

Fig. 11. Velocity of the hydrogen ribbon as function of applied pressure for different temperature of the extrusion nozzle 0.1×1 mm^2.

First laser shots on these solid H_2 ribbons are expected in January 2015 at IoP Prague. The image cross-correlation algorithm will also be improved. It will enable to increase the precision of the velocity measurements by decreasing the error bar down to pixels resolution.

6. CONCLUSION

A cryostat allowing the production of a continuous thin solid hydrogen ribbon was studied and tested at CEA-Grenoble (France). Ribbons of 100 µm and 50 µm in thickness and 1 mm in width were obtained continuously during more than 7 hours at a velocity in the range of 1–14 mm/s. This project enabled to validate a new extrusion concept in which no moving part is used. First results are promising and open several perspectives for the use of solid H_2 targets in miscellaneous field such as protontherapy in medicine or laser-matter interaction in physics. Indeed, even if the 100 µm targets are too thick for TNSA experiments, it enabled to solve technological limitation and leaded to the current thickness of 50 µm, corresponding to the upper limit of the typical thickness for TNSA target (1–50 µm). This technique is currently the only one enabling to continuously produce suitable target for laser experiment. Discussion with IoP team enabled to take into account all the geometric constraints of typical laser setups. First laser shots are expected at the beginning of 2015 at PALS.

7. ACKNOWLEDGMENTS

Authors are grateful to the whole support team working on this project at CEA-SBT Grenoble, and the IoP team (especially Dr. D.Margarone and J.Prokupek) for its future collaboration with the implantation of the cryostat in PALS vacuum chamber. This work is supported by LANEF Grenoble through a LANEF PhD thesis.

REFERENCES

Brenner, C. (2014). High energy conversion efficiency in laser-proton acceleration by controlling laser energy deposition onto thin foil targets. *App. Phys. Lett.* **104**.

Cowan, T. (2004). Ultralow emittance, multi-mev proton beams from a laser virtual-cathode plasma accelerator. *Phys. Rev. Lett*. **92**, 204801–1.

Green, J. (2014). High efficiency proton beam generation through target thickness control in femtosecond laser-plasma interactions. *App. Phys. Lett.* **104**.

Hatchett, S. (2000). Electron, photon, and ion beams from the relativistic interaction of petawatt laser pulses with solid targets. *Phys. Plasmas* **7**, 2076.

Leachman, J. (2010). Thermophysical properties ans modeling of a hydrogenic pellet production system. Mechanical engineering, University of Wisconsin-Madison.

Ledingham, K. (2007). Laser-driven proton oncology – a unique new cancer therapy? *British J. Radiol*. **80**, 855–858.

Maksimchuk (2000). Forward ion acceleration in thin films driven by a high-intensity laser. *Phys. Rev. Lett*. **84**, 4108–4111.

https://doi.org/10.1017/S0263034614000524 Published online by Cambridge University Press

Malka, V. (2004). Practicability of protontherapy using compact laser systems. *Medical Phys*. **31**, 1587–1592.

Malka, V. (2008). Principles and applications of compact laser-plasma accelerators. *Nat. Phys*. **4**, 447–453.

Margarone, D. (2013). Preface: 2nd elimed workshop and panel. *In* A. C. Proceedings (ed.), 2nd MEDical and Multidisciplinary Applications at ELI Workshop and Panel, volume 1546, p. 1, Catania, Itay. ELIMED 2012.

Snavely, R. (2000). Intense high-energy proton beams from petawatt-laser irradiation of solids. *Phys. Rev. Lett* **85**, 2945–2948.

Vinyar, L. (2000). Screw extruder for solid hydrogen. *Techn. Phys*. **45**, 106–111.

https://doi.org/10.1017/S0263034614000524 Published online by Cambridge University Press